

Journal of Biomedical Optics

SPIDigitalLibrary.org/jbo

Development of motion resistant instrumentation for ambulatory near-infrared spectroscopy

Quan Zhang
Xiangguo Yan
Gary E. Strangman

Development of motion resistant instrumentation for ambulatory near-infrared spectroscopy

Quan Zhang,^a Xiangguo Yan,^b and Gary E. Strangman^a

^aMassachusetts General Hospital, Harvard Medical School, Neural Systems Group, 13th Street, Building 149, Room 2651, Charlestown, Massachusetts 02129

^bKey Laboratory of Biomedical Information Engineering of Education Ministry, Xi'an Jiaotong University, Xi'an, Shaanxi, 710049, China

Abstract. Ambulatory near-infrared spectroscopy (aNIRS) enables recording of systemic or tissue-specific hemodynamics and oxygenation during a person's normal activities. It has particular potential for the diagnosis and management of health problems with unpredictable and transient hemodynamic symptoms, or medical conditions requiring continuous, long-duration monitoring. aNIRS is also needed in conditions where regular monitoring or imaging cannot be applied, including remote environments such as during spaceflight or at high altitude. One key to the successful application of aNIRS is reducing the impact of motion artifacts in aNIRS recordings. In this paper, we describe the development of a novel prototype aNIRS monitor, called NINscan, and our efforts to reduce motion artifacts in aNIRS monitoring. Powered by 2 AA size batteries and weighing 350 g, NINscan records NIRS, ECG, respiration, and acceleration for up to 14 h at a 250 Hz sampling rate. The system's performance and resistance to motion is demonstrated by long term quantitative phantom tests, Valsalva maneuver tests, and multiparameter monitoring during parabolic flight and high altitude hiking. To the best of our knowledge, this is the first report of multiparameter aNIRS monitoring and its application in parabolic flight. © 2011 Society of Photo-Optical Instrumentation Engineers (SPIE). [DOI: 10.1117/1.3615248]

Keywords: wearable; near-infrared spectroscopy; laser; tissue oxygenation; parabolic flight; high altitude; motion artifacts.

Paper 10587RR received Oct. 29, 2010; revised manuscript received Jun. 17, 2011; accepted for publication Jun. 22, 2011; published online Aug. 19, 2011.

1 Introduction

Ambulatory near-infrared spectroscopy (aNIRS) refers to the technology that utilizes a wearable near-infrared spectroscopy (NIRS) device for noninvasive, continuous, and long term monitoring of tissue oxygenation and hemodynamics with minimal restrictions on participants' activities. Ambulatory monitoring in general is a rapidly growing domain. Techniques that are currently available include ambulatory electrocardiography (ECG) monitoring,^{1,2} pulse oximetry,³ blood pressure monitoring,⁴ and EEG monitoring.^{5,6} Each of these has its advantages, suitable applications, as well as limitations. Importantly, none of them is capable of directly monitoring tissue blood supply and oxygen consumption changes. For example, ambulatory ECG is used in the diagnosis of syncope by measuring the electric activity of the heart. However, it cannot measure the consequential blood supply and oxygenation changes at the target tissue (e.g., brain). Long term ambulatory monitoring of cerebral blood supply and oxygenation changes could nevertheless provide important supplementary information to ECG Holter monitoring in the diagnosis of syncope.^{7,8} The same reasoning applies when supplementing ambulatory EEG monitoring for seizure detection: seizures are associated with both electrical and hemodynamic changes,^{9,10} whereas EEG measures only neuronal electrical activity. Additional ambulatory monitoring of cerebral blood supply and oxygenation may thus be useful to help diagnose

or manage epileptic patients. Ambulatory pulse oximetry monitoring, used in the study of apnea, provides only arterial blood information; information about venous and tissue blood supply and oxygen consumption¹¹ cannot be measured using pulse oximeters. And some syndromes, for example hemorrhage and hemorrhagic conversion of ischemic stroke, can be effectively monitored only by ambulatory and continuous cerebral monitoring over long-durations.

Further motivation for developing aNIRS comes from the nature of multiple important clinical conditions. A wide variety of medical disorders feature transient symptoms or unpredictable events. That is, the occurrences of critical, diagnostic symptoms, or events can occur unpredictably during patients' normal daily activities, and/or symptom durations are too brief to enable the individual to reach a medical care facility before the symptom recedes. Syncope, smaller strokes, epilepsy, hot flashes, and sleep apnea all fall in this category, and each can be a serious medical condition and a major source of medical costs.¹²⁻¹⁴ Many of the associated transient symptoms generate observable changes in functional, hemodynamic, or metabolic parameters such as tissue blood volume and oxygenation changes, but that dissipate after the event. Thus, development of instrumentation to continuously and unobtrusively monitor tissue blood volume and tissue oxygen consumption could be not only convenient but potentially essential for improved diagnosis, understanding, and management of a wide range of medical conditions.

aNIRS also has the potential to enable several new applications by providing long duration tissue hemodynamics and oxygenation monitoring outside the hospital or clinic environment,

Address all correspondence to: Quan Zhang, Massachusetts General Hospital, Harvard Medical School Neural Systems Group, 13th Street, Building 149, Room 2651, Charlestown, Massachusetts 02129. Tel: (617) 724-9608; Fax: (617) 726-4078; E-mail: qzhang@nmr.mgh.harvard.edu.

with minimal restriction on patients' activity. Examples include at-home sleep studies, on-site evaluation of sports injuries, more comprehensive first-responder emergency medical assessments, supplementary diagnostic information in rural areas, or even hemodynamic assessment in extreme environments including wilderness medicine and spaceflight. The existing technologies (e.g., CT, MRI) are not appropriate for these applications since they are designed for in-hospital, single-shot, or short duration measurements.

The last 30 years have led to substantial progress in noninvasive NIRS and diffuse optical imaging (DOI) technology.¹⁵⁻¹⁸ Several portable NIRS instruments have previously been developed, enabling studies on progressively more mobile subjects in a variety of applications.¹⁷ Runman and Micro Runman developed some 15 years ago in the laboratory of Dr. Britton Chance¹⁹ were pioneering portable NIRS devices, which clearly demonstrated the portability of NIRS and DOI instruments. As another early example, Zhang et al. reported the development of a fully wearable, battery powered microcontroller-based NIRS system.²⁰ This system was designed for hematoma detection in settings where other imaging modalities, such as CT, were unavailable. More recently, a commercially available system, Infrascanner (InfraScan, Inc.) was developed for hematoma detection, based on the differential light absorption of the injured versus the noninjured part of the brain.²¹ With this system, an operator holds a wireless probe over the region of interest during measurements. So far, the most widely reported aNIRS system is the HEO-200 (OMRON, Japan), with single source-detector pair, 2 Hz sampling rate and up to 6 h of monitoring time. HEO-200 has been used in several functional studies of brain and muscle²²⁻²⁵ and is capable of both wireless and wired operation. More recently, Wolf et al.^{17,26} reported the application of a wireless NIRS device for monitoring brain function, with four sources, four detectors, a 100 Hz sampling rate (a factor of roughly 10 to 100 higher than previous devices), and a 3 h battery life. In addition, a commercially available, single-channel wireless system, PortaMon, monitors muscle tissue oxygenation for up to 10 h.²⁷ When more channels are implemented and the spatial coverage improved, ambulatory diffuse optical imaging (aDOI) can be achieved. Finally, Atsumori et al. reported the development of a wearable optical topography system for mapping the prefrontal cortex activation.^{28,29} With eight source location (two wavelength) and eight detectors, the entire forehead can be covered and functional brain imaging at a 5 Hz frame rate is possible.

Despite these achievements, a number of substantial gaps remain. The first is a capability for unrestricted ambulatory monitoring. While wireless communication enables real time display and monitoring of the collected data, the range of the subjects' activities is typically limited to an area less than approximately 10 m radius inside the building. Second, long-duration continuous recording capabilities greater than 10 h remain to be developed. Third, none of the available systems have a multimodality recording capability to enable correlation with other physiological or external events. Fourth, and perhaps most important, methods to improve aNIRS systems' resistance to motion during subjects' normal activity still need to be studied. This leaves ample room for further development and applications of aNIRS, and aDOI, particularly in terms of enabling patient mobility and truly long-duration monitoring. Considering the

needs from potential applications such as syncope, epilepsy, and sleep monitoring, an ideal aNIRS or aDOI device 1. should not limit the subjects' activities or range of the subjects' movement; 2. should provide greater than 8 h of continuous recording time; 3. should be capable of sampling rate of 20 Hz or greater, as functional hemodynamics has a typical bandwidth of about 5 Hz, and to avoid aliasing and separate cerebral signal and systemic interferences (such as cardiac activity); 4. should provide multichannel monitoring to enable comparison between healthy sides and pathological parts of the body, or help reduce systemic interference;³⁰⁻³² 5. should have multimodality monitoring capability (e.g., electrocardiography, or respiration, or to synchronize with external devices) to enable both redundant and synergistic measurements of symptoms that have multiple physiological effects; and 6. critically, an optimal aNIRS system must be fundamentally designed around providing strong motion artifact reduction and/or identification during ambulatory monitoring. aNIRS by definition involves substantial subject motion, and hence artifacts associated with such motion need be minimized. Indeed, from our experience, as well as others,¹⁸ a major challenge in ambulatory NIRS monitoring is how to handle motion artifacts. Our approach is to minimize artifacts as much as possible via instrument design, and simultaneously acquire relevant information for effective post-acquisition artifact reduction.

From the technology development point of view, aDOI faces the same important challenges aNIRS faces: reducing device size, minimizing power consumption, and dealing with the inevitable motion artifacts in an ambulatory setting. Limited by the capacity of the battery, currently there is a tradeoff between continuous monitoring time and spatial coverage. While an aNIRS device has fewer channels and hence less spatial coverage, it is generally capable of a higher data acquisition rate, lighter weight, more comfortable probe, and it can often achieve much longer monitoring times. These advantages make aNIRS particularly suitable for continuous long term monitoring, especially in contexts that involve substantial motion. On the other hand, aDOI is necessary when spatial features of the contrast are needed in the application.

With the ultimate goal of developing wearable neuro-monitoring for astronauts during spaceflight, we have begun developing a series of aNIRS instruments. Ambulatory performance tests have included ambulatory monitoring during parabolic flight and in extreme and remote environments (e.g., high altitude hiking on Mt. Kilimanjaro). In this paper, we present the development of the novel multichannel and multiparameter aNIRS device where we sought to reduce the motion artifact by utilizing lightweight system design, motion-resistant probe design, and also integration of motion sensor. With these motion artifact reduction techniques, our initial results suggest that it is possible to reduce motion artifact even in fairly extreme nonlaboratory conditions and still acquire high quality aNIRS measurements. This paper focuses on the hardware development.

2 Motion Resistant aNIRS Instrumentation Design

2.1 General Description/Features

The NINscan (Near-INfrared SCANner) system is shown in Fig. 1. This fully wearable system consists of an optical probe,

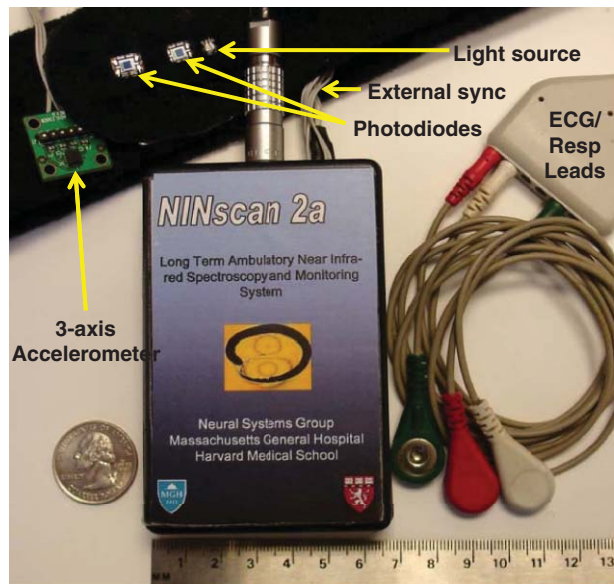


Fig. 1 NINscan, a second generation aNIRS device, designed to minimize motion artifacts. This system has 1. four optical channels via a dual wavelength light emitting diode (LED) source, and two photodiode detectors, 2. one ECG channel, with the three leads shown at right, 3. one active impedance respiration channel, which also uses the ECG leads, and 4. two motion sensing channels, selected from a tri-axial accelerometer.

three ECG/respiration chest electrodes, a motion sensor, an external synchronization line, and a wearable recorder with onboard data storage. NINscan has four optical channels to measure tissue hemodynamics and oxygenation level, one differential ECG channel, one respiration channel, and two accelerometer channels. To minimize restrictions on subject activities, NINscan does not use wireless communications for data transfer to a separate station; instead, all data acquired are stored in 512 M byte of on-board memory. Powered by 2 AA size lithium batteries, NINscan can monitor tissue hemodynamics and oxygenation, ECG, respiration, and subjects' motion simultaneously and continuously for up to 14 h at 250 Hz sampling rate. In addition, when working with other physiological monitoring devices (such as pulse oximeters), an external synchronization timing signal can be exported so that NINscan can be synchronized with auxiliary devices or recordings. When data acquisition is complete, NINscan is connected to a computer via USB2 for data download and analysis. The detailed specifications of NINscan can be found in Sec. 3.1 and Table 1.

2.2 Structure of the aNIRS Prototype

The functional diagram of NINscan is shown in Fig. 2.

NINscan can use multiwavelength light-emitting diodes (LEDs) or laser diodes (LD) for light sources. Single-package multiwavelength LEDs and LDs are becoming more readily available, in a growing selection of red and near-infrared wavelengths, ideal for aNIRS applications. (For example, dual-wavelength red and near-infrared high power LDs from Axcel Photonics Inc, Marlborough, Massachusetts; LEDs from Epitex, Inc, Kyoto, Japan.) The advantages of using multiwavelength single package light sources are clear. First, such sources provide less positional error: a single package light source ensures

Table 1 Basic specifications of NINscan.

Dimensions	65 mm × 120 mm × 15 mm
Weight	350 g (including batteries)
Working current/power consumption	160 mA/0.48 W
Sampling rate	250 Hz
A/D converter bit depth	12 bits
Onboard memory	512 M byte
Number of channels	8 (4 NIRS/1 ECG/1 respiration/2 accelerometry)
Battery life (2 AA size Lithium batteries)	14 h
Bandwidth of optical channels:	0 to 5 Hz
Bandwidth of ECG	0.1 to 40 Hz
Bandwidth of respiration:	0.03 to 0.7 Hz
Bandwidth of motion:	0 to 50 Hz

overlapping source positions for different wavelengths, thus reducing the error in spectroscopy analysis due to positional error. Second, probes designed with fewer parts are lighter and smaller, and hence more resistant to motion artifact. Third, multiwavelength sources provide more robust measurements: when the different wavelengths are packed in the same diode instead of different packages, the motion artifact due to light source movement will be close to common mode interference to signal acquired at different wavelengths, making it easier to identify and cancel using signal processing algorithms.

For detection, NINscan uses two monolithic photodiodes as detectors (OPT101, with on-chip transimpedance amplifier; Burr-Brown Inc, Tucson, Arizona), and hence can monitor tissue at two separate locations. The two detectors are typically configured as a multi-distance probe,³⁰⁻³² with the near detector sensing systemic physiological fluctuations and motion artifacts, and the far detector additionally measuring deeper tissue hemodynamics and oxygenation measurement. The optical channels work in frequency division multiplexing mode at approximately 1 and 8 kHz modulation, so that the signals from the two light sources can be separated and the ambient light can be rejected. Once the lights at two modulation frequencies pass through the tissue and are detected by the detectors, they are separated by band pass filters (BPF1 and BPF2 in Fig. 2), demodulated, and then amplified. To reduce the noise, a 22 Hz low pass filter is put at each detector channel before the signal is digitized and sampled into the memory. A calibration procedure is required to correct any signal offset (such as dark current).

In addition to the four NIRS channels, NINscan also has one ECG channel, whose quality is equivalent to that found in standard ambulatory electrocardiography (Holter monitoring), and one bio-impedance-based respiration channel. A low-intensity 62.5 kHz current is injected into two electrodes and the voltage, which represents the respiration induced impedance change, is

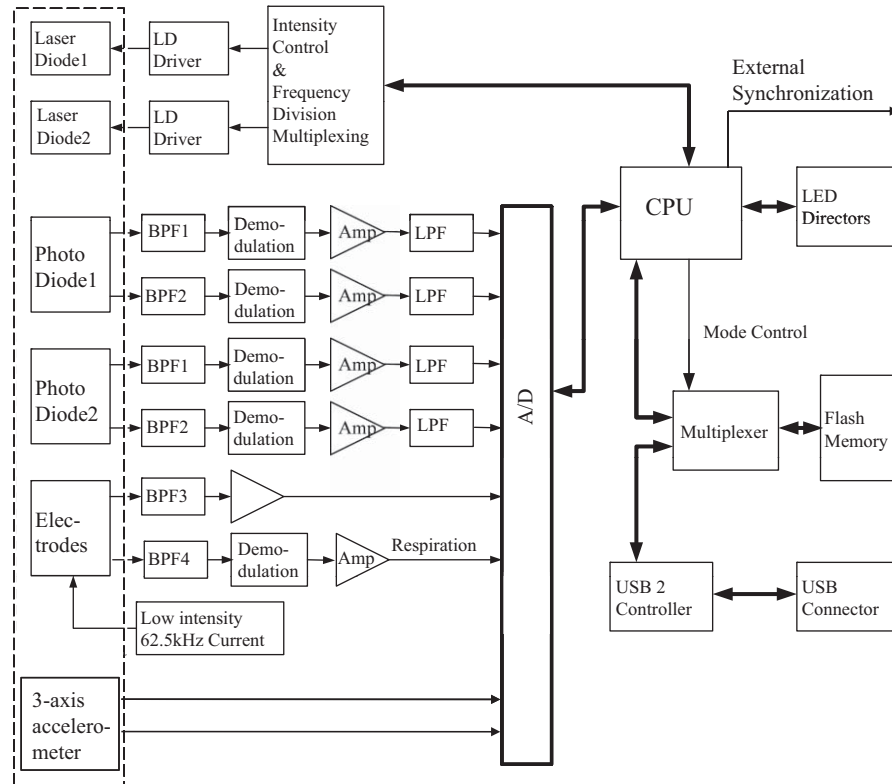


Fig. 2 Functional block diagram of NINscan. The dashed line represents components contained within the external probe.

picked up at the same electrodes. The ECG and respiration channels share three chest electrodes, with the signals separated by the two band pass filters, BPF3 and BPF4 in Fig. 2. The ECG signal is then fed to a differential amplifier. The bandwidth of the ECG is set at 0.1 to 40 Hz; the 0.1 Hz lower cut off frequency is to eliminate baseline drift, while the 40 Hz high cut off frequency is to remove line noise interference. The respiration signal is extracted by the BPF4 with pass band of 60 to 65 kHz; it is then demodulated, converted by the analog to digital (A/D) converter, and stored in the on-board memory.

NINscan also has two motion sensing channels, based on a low power, 3-axis accelerometer (ADXL330, Analog Devices, Inc.) with an acceleration sensing range of ± 3 g. Since there are only two additional channels available for motion monitoring, we custom-select two axes of subjects' movement for monitoring depending on the application.

The system is controlled by a low power MSP430 family microcontroller. All eight analog signals are strictly co-registered, digitized by a 12 bit A/D converter and sampled at 250 Hz. To allow synchronization of NINscan with other patient monitoring devices, a periodic trigger signal is exported through an external synchronization line. As part of the user interface, LED indicators are used to indicate the working status of the device. The system operates in two modes: recording mode and transfer mode. In recording mode, the CPU stores samples in its 512 M byte flash memory in FAT16 file format. When the recorder is connected to a computer via USB2, the device is automatically recognized as an external disk and the system automatically enters transfer mode to enable data file copying, where 10 h of recording can be downloaded in less 60.

2.3 Motion-Resistant System Design Considerations

Four primary features were integrated into NINscan to help minimize motion artifacts. First, we sought to minimize the NINscan device size using surface mount technology, optimized multilayer PCB design, and a customized chassis. The resulting device fits into a $65 \times 120 \times 15$ mm space, about the size of a person's palm, and weighs only 350 g (including batteries). Second, lightweight and flexible wires connect the optical probe and chassis. These replace the typical heavy, stiff and/or fragile optical fibers, and dramatically reduce tether forces on the probe, also helping minimize motion induced probe shift. Third, we integrated a motion sensor into the probe itself. While accelerometer-based motion information is important in many studies (e.g., evaluation of sleep disorders), it is also useful in the identification and reduction of motion artifact in the optical channels. For example, we have begun to utilize adaptive filtering artifact reduction methods for motion reduction³³ with preliminary tests suggesting that this approach can reduce the motion artifacts by 70% or more.³⁴ Fourth, we have sought to minimize the mass of the optical probe itself and incorporated several design features to minimize motion susceptibility, as discussed next.

2.4 Motion Resistant Probe Design

Probe design is key to reducing motion artifacts. The structure of our current probe is shown in Fig. 3.

As seen in Fig. 3(b), the light source and the two optical detectors are installed on small pieces of circuit board, then

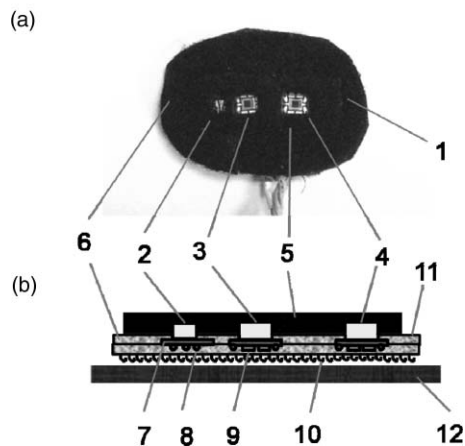


Fig. 3 Structure and positioning of a NINscan probe. (a) photo of the probe pad. (b) structure of the probe and the soft fixation band (side view). 1. Probe. 2. Dual wavelength light source. 3. First optical detector. 4. Second optical detector. 5. Black filling material. 6. Probe base material. 7. Circuit board. 8. Leads and wires. 9. Electronic components on the circuit board. 10. Velcro bottom surface. 11. Adhesive top surface. 12. Fixation band.

embedded in the probe base pad, which is made by two layers of black, flexible material. For the probe shown in Fig. 3, the source-detector separations are 1.3 cm and 2.5 cm, respectively. The optical source and detectors are located at the center of the pad and about 2.5 cm from the edge. In this way, most of the ambient light will be blocked by the pad and hence will not affect the optical measurements. The light source and detectors are surrounded by soft and elastic filling materials that prevent light leakage from the source directly to the detector. The whole probe in Fig. 3(a) is secured to a soft, black, elastic band, which then wraps around the subject's head. The back of the probe uses a Velcro surface for secure adhesion to the band. The positioning of the probe is shown in Fig. 3(c), including an embedded motion sensor, with a total mass of only 15 g. While the OPT101 can handle high optical flux, when the ambient light is extremely bright (e.g., outdoors at high altitude), a light blocking cap can help reduce the potential for detector saturation due to ambient lighting conditions.

From our experience, the following concepts in the probe design improve its motion resistance. First, the probe (including all cabling) must be lightweight to minimize tether forces and thus reducing the possibility of probe position changes during movement. To achieve this, the optical sources and detectors have been directly integrated into the probe so that the typical heavy optical fibers can be replaced with lightweight, flexible wires. Second, the probe, or portions thereof, can be made to adhere to the skin to secure its position and reduce the possibility of it shifting. Third, the shape of the probe is preformed to the curvature of the target tissue. Fourth, black filling material must be used to prevent light leakage from the source directly to the detector without going through the tissue. Fifth, if applicable, a black cover should be placed over the probe to block environmental lights and further reduce the possibility of detector saturation. In addition, the two detectors can be configured as multidistance, so that the motion interference, which is common to both detectors, can be then removed by signal

processing, for example adaptive filtering based algorithm.^{30–32} Above all, maintaining subject comfort is critical—an otherwise perfect probe can be easily foiled by an uncomfortable subject. Total probe mass is key here, in addition to the elimination of any sharp edges or pressure-points.

2.5 Data Analysis Algorithms

NINscan is a continuous wave instrument, thus absolute measurements of tissue hemodynamics and oxygenation level cannot be acquired without assumed tissue baseline optical properties, or measurement of baseline optical properties using frequency domain or time domain instruments. To convert optical measurements to relative changes in the concentration of deoxy-hemoglobin (HHb) and oxy-hemoglobin (O₂Hb), we use the modified Beer–Lambert Law.^{35–38} The raw 250-Hz optical data are offset-corrected and further digitally low pass filtered at 5Hz (in addition to the instrument filter). The differential path length factor (DPF) used in the calculations can be based on Monte Carlo simulations with common head structure and tissue optical properties.³² When multisource-detector separation configuration is used, adaptive filtering based common mode interference cancellation can be applied.^{30–32}

3 Performance Tests

3.1 Instrument Characterization

The detailed specifications of the NINscan system are shown in Tables 1 and 2. NINscan's internal memory can store data from 8 channels at 250 Hz sampling rate up to 36 h, while its low power consumption (0.48 W) allows the system to run up to 14 h continuously from with 2 AA size lithium batteries (the recording time can be extended with added parallel battery pack). The bandwidth of each channel is designed according to the characteristics of each parameter. For example, ECG has 0.1 to 40 Hz bandwidth, commonly used in ambulatory electrocardiography, whereas the NIRS channels have a 0 to 5 Hz bandwidth. Although different parameters have different bandwidth requirements, they are all sampled at 250 Hz to enable strict co-registration between signals. Table 2 summarizes the major characteristics of the optical channels, the core of aNIRS monitoring. For battery powered long term ambulatory monitoring, signal drift is a critical parameter, since the voltage of

Table 2 Basic specifications of the optical channels.

Noise equivalent power	15 pW/ $\sqrt{\text{Hz}}$
Instrument dynamic range	55 dB
Drift (stability)	0.02%/h
Linearity	5%
Crosstalk	–40 dB (1%)
Light power	<5 mW
Wavelengths	variable (660 to –910 nm)

the battery decreases significantly as its power is consumed and it is important that the signal channels are resistant to the battery voltage change. For NINscan, the average drift is about 0.02%/h, excellent for our long term monitoring application. The noise equivalent power (NEP) of NINscan was found to be $15 \text{ pW}/\sqrt{\text{Hz}}$, including both the dark noise from the OPT101 detector (about $5 \text{ pW}/\sqrt{\text{Hz}}$) and the noise from the electronic circuit that follows. This NEP value is roughly 15 times higher than that of avalanche photodiode-based instruments.³⁹ NEP determines the minimum light an optical instrument can detect, which consequently determines the maximum source-detector separation on the subject (about 2.5 cm in our applications). The 55 dB dynamic range refers only to the recorder and does not include the sensor whose gain can be optimized and adjusted according to the source-detector separation or the subject difference.

Either dual wavelength laser diodes or LEDs can be used as light sources. Currently there are many commercially available dual-color or multicolor LEDs or LDs, with flexibility in the choice of appropriate power and wavelengths. For NINscan we choose dual color LEDs or LDs with wavelengths ranging from 660 to 910 nm. For the tests in this paper, a dual color LED (660 and 905 nm) is used as the light source. Although laser diodes can easily generate high incident light power thus probe deeper tissue, the actual power applied is regulated by the maximum permissible exposure from laser safety standards, and it depends on the wavelength and area of the laser illumination spot.⁴⁰ While the wide bandwidth of LEDs will introduce error in spectroscopy analysis, to a certain extent this error can be reduced by using “effective extinction coefficient.”⁴¹ Coupled with their small size, low cost and robustness, LEDs are still a practical choice in aNIRS monitoring.

3.2 Long Term Quantitative India Ink Titration Phantom Test

In order to test the long term stability and quantitative accuracy of NINscan, we performed multiple 14-h ink titration phantom tests. The phantom consisted of a container filled with 2000 ml of 0.5% intralipid, sitting atop a magnetic stirring stage (IKA C-MAG MS 7, IKA Works, Inc, Wilmington, North Carolina) and continuously stirred to ensure the homogeneity of the solution. Droplets of black India ink solution (Design Higgins, Sanford, Bellwood, Illinois) were titrated into the solution at a constant speed over 14 h of titration time. The titration speed ranged from 0.02 to 0.06 ml/hour, controlled by a high accuracy syringe pump (KD Scientific, Inc, Holliston, Massachusetts). The total titration volume of the ink solution over 14 h was less than 1 ml, therefore the ink titration changed the phantom absorption properties (linear to titration time), but did not affect the scattering property of the phantom. Multiple tests with different amounts of ink solution were performed to simulate different tissue optical properties. The phantom was monitored using battery powered NINscan for the entire titration period; after the titration, the absorption coefficient of the phantom was calculated using the modified Beer–Lambert law (assuming constant scattering properties). Results from two titration tests, one to simulate fatty tissue and one to simulate more absorbing (i.e., more vascularized) tissue, are shown in Fig. 4.

As we can see from the results, the absorption coefficient of the two titration tests increase linearly with titration time (the steps represent the falling and mixing of the discrete ink droplets during titration), which is proportional to the concentration of the ink, since the titration rate is constant. Regression analysis shows that the absorption coefficient and the titration time (or ink concentration) are highly co-linear, with a Pearson correlation

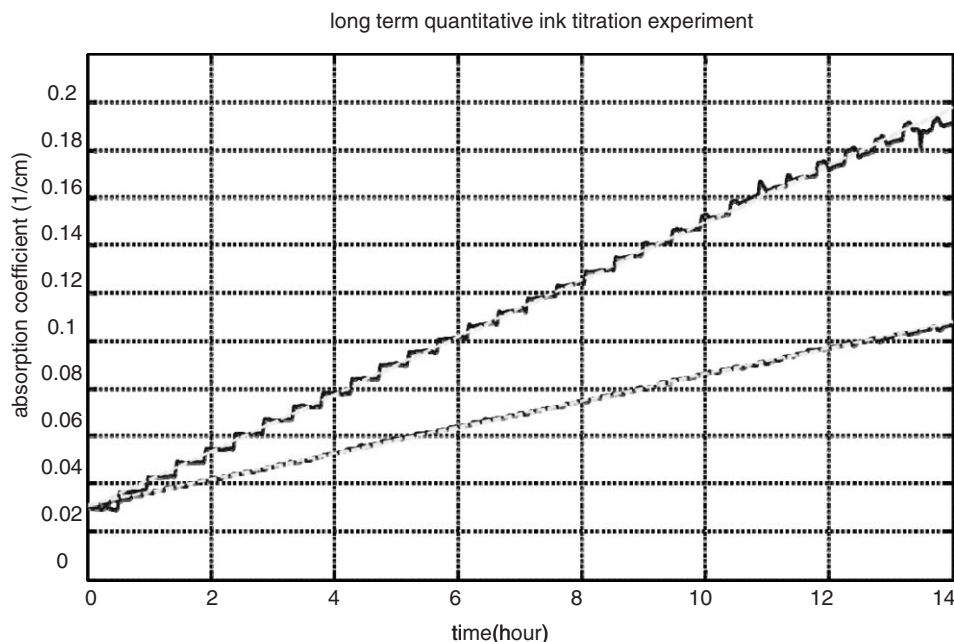


Fig. 4 Results from two long term ink titration phantom tests to demonstrate the stability and quantitative accuracy of NINscan. The top curve is from an India ink titration test (at constant titration speed) simulating dark tissue types and the bottom curve is from a phantom test simulating light tissue types. The black solid lines are the absorption coefficients calculated from NINscan measurements, and the gray dashed lines are their linear fitting results. The steps in the curve show the falling of the ink droplets into the intralipid solution, which was continuously mixed to maintain a homogeneous phantom.

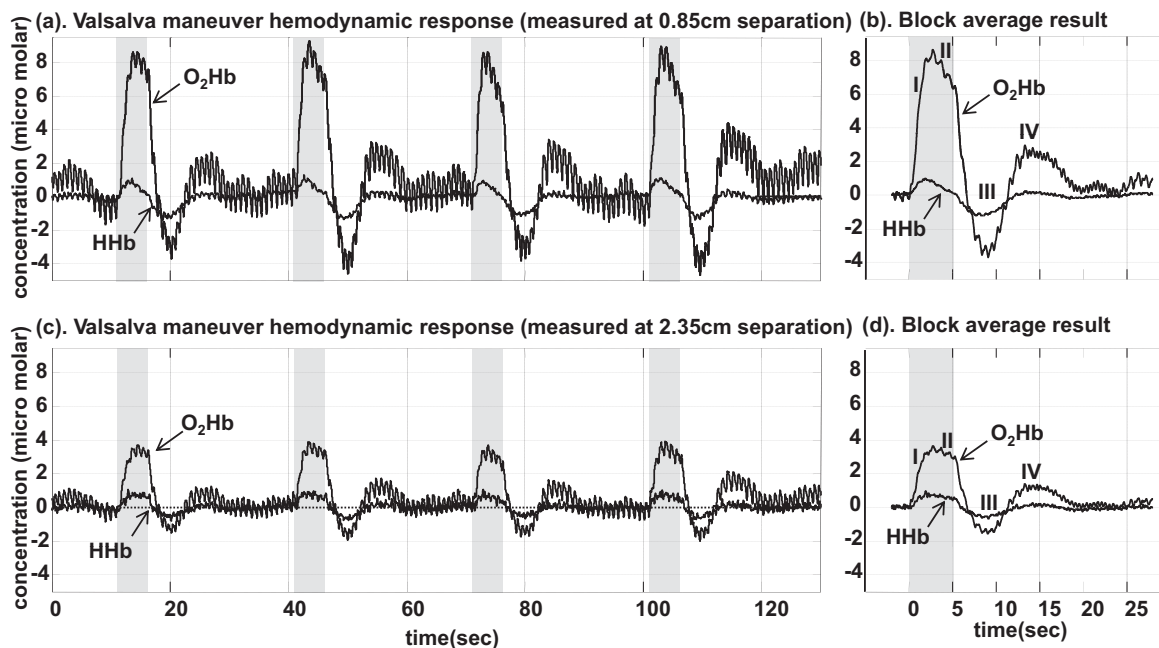


Fig. 5 Valsalva Maneuver hemodynamic response measured using NINScan. (a) O₂Hb and HHb measurements from a detector 0.85 cm from the source, and (b) its block averaged result. (c) O₂Hb and HHb measurements from the detector 2.35 cm from the source, and (d) its block averaged result. The four phases I, II, III, and IV of Valsalva maneuver are clearly demonstrated (see text).

coefficient $r > 0.999$, and $p < 10^{-20}$. The optical properties of the solution were calibrated using the radio frequency and continuous wave NIRS systems as in our previous studies,^{30–32,39} and the results calculated from NINScan agree well with the calibration measurements. In practice, a DPF needs to be applied when a modified Beer–Lambert law is used for cw to calculate the absorption coefficients.^{30–32} Here a DPF of 7.6 was used to calculate the absolute absorption values.

3.3 Valsalva Maneuver Test

Valsalva maneuvers are widely used to test for cardiac function and autonomic nervous system function,^{42,43} and are performed by forcible exhalation against a closed airway. Valsalva maneuvers provide strong hemodynamic changes, and are often used to test the quality of NIRS measurements.

A healthy male subject was seated with the NINScan 2a probe placed over the right forehead just below the hairline. The Valsalva maneuver was executed four times for a duration of 5 s, interleaved with intervals of 25 s of rest. The total acquisition time was 120 s.

Figure 5 reveals the measured, and expected, hemodynamic response to the Valsalva maneuver. Displayed are both the full time course and the block average for four Valsalva events from both the close detector and the far detector. The protocol produced clearly reproducible responses to each stimulus, including all four phases of hemodynamic change during a Valsalva maneuver.^{42,44} As shown in the block average diagram, at phase I, there is a strong increase in oxygenated hemoglobin concentration and smaller increase in HHb, due to transient increase in the arterial blood pressure, thought to result from transmission of the intrathoracic pressure to the arterial tree during the maneuver. In phase II, the O₂Hb and HHb concentrations decrease

because of a fall in the arterial blood pressure, ABP (due to impaired atrial filling of the heart). When the strain is released, the sudden decrease in intrathoracic pressure is again transmitted to the arterial system and a transient decrease in ABP occurs, resulting in the sudden decrease of O₂Hb and HHb concentration, as shown in phase III. This is followed by a phase IV, an overshoot in ABP and O₂Hb and HHb, above baseline, as the sympathetic tone and systemic vascular resistance remain elevated, after atrial filling has normalized. The strong hemodynamic responses acquired from the close detector and from the far detector are similar, since the blood pressure changes produced by Valsalva maneuver are systemic. The Valsalva maneuver tests validate NINScan's capability for tissue hemodynamic measurements.

3.4 aNIRS During Parabolic Flight

The Valsalva maneuvers do not require, and did not involve, participant motion. However, aNIRS recording by definition involve motion. One context which makes use of both the ambulatory monitoring and motion sensing capabilities of our NINScan aNIRS device is flight in an aircraft. Various flight trajectories, particularly in high performance aircraft, can induce substantial shifts in cerebral perfusion, with high-g maneuvers being capable of inducing unconsciousness.^{45,46} Parabolic flight trajectories, in contrast, allow simulation of the microgravity conditions experienced in spaceflight. As an initial investigation of systemic and cerebral hemodynamics relevant to spaceflight, a single 32 year old, healthy male was fitted with our NINScan device prior to boarding a parabolic flight (Fig. 6). The accelerometer was mounted in the head probe, as shown in Fig. 7(a), and the participant sat upright facing the cockpit during the measurements. This aligned the acceleration sensor axes



Fig. 6 *In vivo* hemodynamic monitoring using aNIRS during parabolic flight. Wearing NINscan, the subject went through six parabolas simulating the gravity on Mars, six parabolas simulating Lunar gravity, and four parabolas simulating spaceflight. The systemic and cerebral hemodynamics were monitored continuously during the flight, together with simultaneous re-registered acceleration, respiration and ECG. [The authors have written permission to show the participant's face.]

with the anterior–posterior (G_x) and superior-inferior (G_z) axes of the plane. aNIRS and synchronized accelerometer recordings were started on the ground prior to liftoff and continued until after landing. While the participant remained seated, the

plane flew two sets of three parabolas simulating the gravity on Mars, two sets of three parabolas simulating Lunar gravity, and a set of four parabolas simulating spaceflight microgravity. Calculation of an estimated gravitational vector from the dual-axis accelerometer data was accomplished by assuming the third (left-right) axis provided zero contribution to the gravitational change (i.e., assuming the subject's head remained facing forward and upright throughout the flight, as the participant was instructed). The NINscan accelerometer recordings are shown in black in Fig. 7(b). A separate tri-axial accelerometer mounted on the plane body recorded three datasets, during Mars, Moon, and microgravity periods. The close correspondence between the two, both filtered to a 10 Hz bandwidth, is shown in Fig. 7(b), with detail in the inset in Fig. 7(c).

To monitor changes in blood volume associated with periods of microgravity and hypergravity, the hemodynamic measurements, synchronized with the accelerometer recordings, were collected by NINscan from the left forehead immediately anterior to the accelerometer [rectangle, Fig. 7(a)]. Signals were converted to O_2Hb and HHb via the MBLL and summed to obtain total hemoglobin (HbT). HbT results are shown in Fig. 8, revealing clear and repeatable increases in blood volume during periods of microgravity from both near and far sensors, corresponding to the known cephalic fluid shifts during microgravity. These increases begin to normalize later in the approximately 25 s freefall and are followed by clear and repeatable decreases in HbT associated with periods of hypergravity (up to approximately 1.9 g). Despite the substantial motion associated with parabolic flight, our recordings demonstrated no observable motion artifacts in the NIRS signals, and provided evidence of sensitivity to cerebral hemodynamics in such settings.

To our knowledge this is the first published report of the use of NIRS to monitor systemic and cerebral hemodynamic

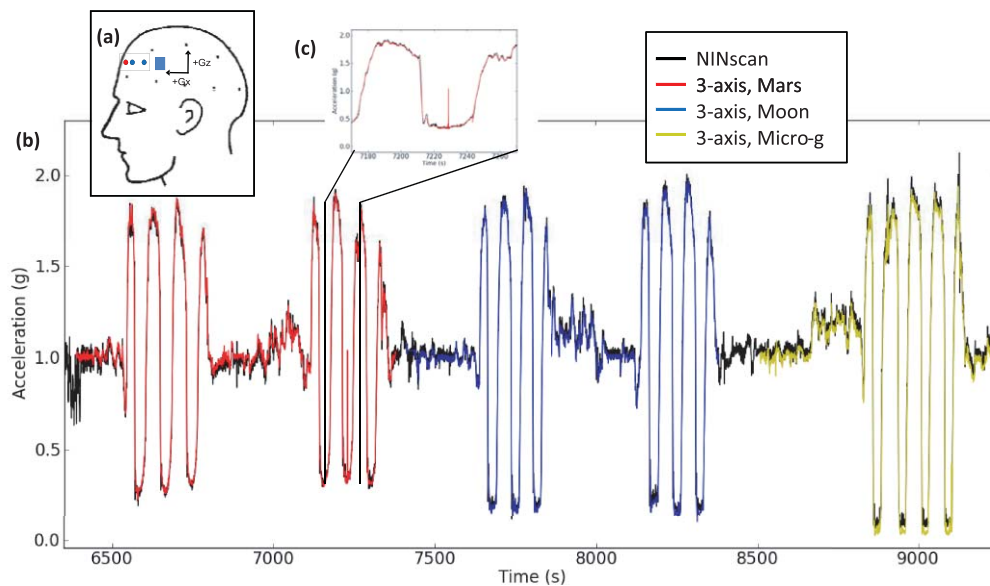


Fig. 7 Accelerometer recordings during parabolic flight. (a) Position of the accelerometer (blue square) in relation to the participant's head. (b) Continuous NINscan accelerometer estimate of gravitational loads during parabolic flight (black) with an overlay (colors) of the aircraft-mounted tri-axial accelerometer trace showing close correspondences throughout the flight and low-gravity periods approximating Martian gravity (red), lunar gravity (blue) and microgravity (yellow). (c) Expanded view to demonstrate the details.

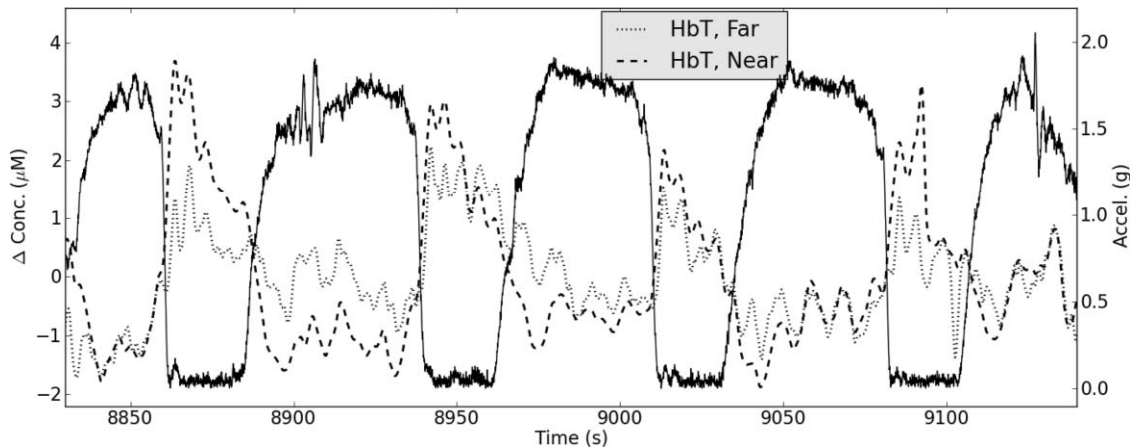


Fig. 8 Example changes in total hemoglobin (HbT) recorded at near and far detectors (1.1 and 2.5 cm, respectively) during parabolic flight are shown in dotted and dashed lines. Solid line represents the acceleration profile recorded by the NINscan accelerometer (scale on the right-hand y-axis).

parameters during parabolic flight. The parabolic flight shows that with careful motion-resistant system design, it is possible to overcome the motion artifact and acquire high quality aNIRS measurements.

3.5 aNIRS During High Altitude Hiking

In order to further evaluate NINscan's resistance to motion in realistic environment on subjects with substantial activities and motion, we used NINscan to monitor healthy participants during unrestricted mountain hiking up Mt. Kilimanjaro. Multimodality NINscan recordings from a subject hiking at an altitude of approximately 4000 m, along with an assessment of motion resistance, are shown in Fig. 9.

Figure 9(a) shows all parameters that were synchronously recorded by the device over a 5 min period, including four optical channels, ECG, respiration, and two accelerometry channels. These data were from a 4 h recording; plotting more data obscures the individual waveform details. The periodic bumps in the black accelerometry channel correspond to individual foot-falls while hiking. From multiple previous studies,^{30–32} there is known to be a close relationship between near and far sensors (sensitive to shallow and deeper tissues, respectively). This is depicted in Fig. 9(b) which plots the near versus far 905 nm signals. Linear regression gave a highly significant Pearson correlation coefficient $r = 0.89$ (slope = 0.65; $p \ll 10^{-10}$). In contrast, Fig. 9(c) shows the relationship between the motion (e.g., footsteps measured by the accelerometer) and optical traces, after normalizing each into the range 0 to 1 ($r = 0.03$, slope = 0.014, $p > 0.05$). Thus, a full-scale excursion in the accelerometer generated no nonsignificant change in the optical trace. This compares quite favorably with typical fiber-based systems which can generate upwards of 20% to 50% or larger changes in optical signals with similar motion inputs.

The high altitude hiking data and associated correlation analysis provide a quantitative assessment of NINscan's resistance to motion in realistic test environments, and also demonstrates the robustness of our NINscan device to harsh environments.

4 Discussion

This work has described the design, characterization and applications of a new aNIRS device, called NINscan, for long-duration, mobile monitoring of tissue hemodynamics and oxygenation. The laboratory and human experiments described support the accuracy of the device, as well as its suitability for use in various mobile, remote, and even extreme environments.

4.1 Applications of aNIRS

Ambulatory ECG monitoring paved the way for a new subfield in cardiology and has become a routine procedure for detection and diagnosis of many disorders characterized by intermittent or rare cardiac symptoms (e.g., arrhythmias, transient ischemic episodes and silent myocardial ischemia).^{1,2} We sought to develop aNIRS systems to similarly open up new domains to hemodynamic monitoring. By also incorporating standard ECG, respiration and motion monitoring, NINscan has significant potential in the diagnosis, monitoring and management of many diseases related to abnormal cardiovascular status, tissue hemodynamics and oxygenation levels. While it is difficult to predict the most promising applications, we expect aNIRS to provide information complementary to that currently available via ambulatory recording modalities. Such data is relevant to a wide variety of health problems where suffering and health care costs are significant. For example, one million patients are evaluated for syncope in the U.S. annually; it can be highly disabling and is further associated with a risk of sudden death.¹² The tissue blood supply and oxygen consumption data collected during patients' daily activity by aNIRS may help improve the diagnosis efficacy and accuracy, and reduce the associated cost. Similarly, with over 180,000 people diagnosed with epilepsy⁴⁷ each year, it is possible that aNIRS monitoring could 1. help enable early detection and/or intervention for epileptic seizures, 2. improve or speed-up treatment evaluation, and 3. enhance the objectivity of epilepsy severity evaluation. Furthermore, approximately 150,000 deaths/yr are attributed to stroke¹⁴ and about 9.7% of acute ischemic stroke have secondary hemorrhagic conversion. aNIRS and aDOI monitoring may eventually reduce the need for repeated CT scans, and consequently reduce radiation

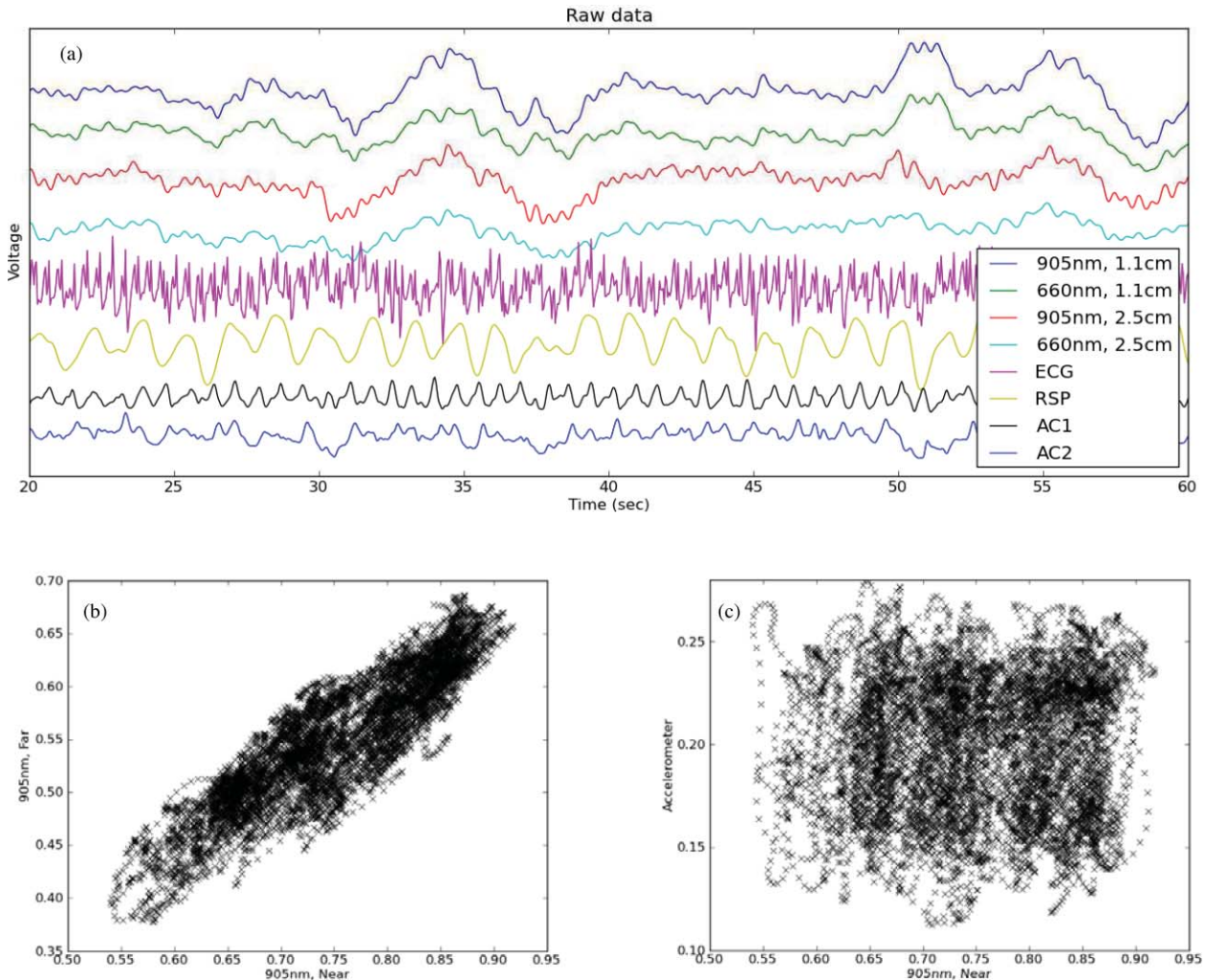


Fig. 9 Multiparameter NINscan monitoring during high altitude hiking on Mt. Kilimanjaro. (a) Parameters that were synchronously recorded by the device included four optical channels, ECG, respiration, and two accelerometry channels. (b) Correlation between optical channels. (c) Correlation between motion and optical measurements.

and cost, improve safety and comfort. Sports medicine, rural medicine, wilderness medicine, and aerospace medicine may also benefit from a highly portable method for monitoring tissue oxygenation.

4.2 Ongoing and Future Development

Technology development of NINscan for long term, continuous, multichannel aNIRS functional monitoring demonstrated several challenges beyond those for ambulatory ECG monitoring. These include low power consumption and low noise electro-optical system design. ECG monitoring is a passive recording method, whereas aNIRS requires light sources to illuminate the tissue. For battery operated continuous long term monitoring devices, therefore, high current light sources not only challenge power consumption and battery life, but can also introduce significant noise to the detection circuitry, particularly when measuring weak signals coming from deep tissue. However, motion artifacts remain the most important challenge. Handling of motion artifacts in dynamic ECG monitoring is well established,⁴⁸ however, methods to reduce and treat motion artifacts in aNIRS

or aDOI are still under development. Without proper handling of motion artifacts during ambulatory monitoring—ranging from prevention to identification and reduction—the use of aNIRS will remain significantly restricted.

Besides addressing the issue of motion artifacts, other difficulties associated with aNIRS monitoring also need to be addressed. In recent work, we have sought to separate the effect of fluctuations in systemic hemodynamics, since active ambulatory subjects will necessarily generate changes in systemic blood pressure, blood flow, heart rate, respiration rate, and more.^{30–32} In addition, we currently use photodiodes for detectors. While a photodiode can support a wide range of applications at high light flux, the sensitivity of a simple photodiode is limited. For deep tissue applications such as cerebral monitoring, it would be preferred for aNIRS to have higher detection sensitivity and bandwidth capability, potentially provided by custom detectors based on avalanche photodiodes. Smaller, but nevertheless important, advancements under development include tri-axis accelerometry, user buttons to mark external events, and source time-sharing to reduce power requirements.

4.3 Summary

Over the past several years, a major goal for our efforts has been to develop a portable neuro-monitor for use outside the confines of a hospital, and more specifically to develop a capability for evaluating astronauts during spaceflight. We are also driven by the broad clinical applications of this technology. NINscan represents our first step toward small, lightweight aNIRS devices with low power consumption, high performance and most importantly, motion resistance. This is an important step forward based on existing portable or bench side NIRS instruments, and we believe this design will aid in the development of aDOI systems with similar features.

In conclusion, aNIRS is a promising technology and we have demonstrated that a major source of interference in continuous long term aNIRS recording—namely, motion artifacts—can be reduced to an acceptable level with light weight system design and motion resistant probe design. Once proven feasible and effective for clinical applications, the benefits of aNIRS will include the potential for improved safety (no ionizing radiation), efficiency for catching unpredictable events, comfort, reduced obtrusiveness, and potentially reduced health care cost, and reduced morbidity or mortality.

Acknowledgments

This work was supported by the National Space Biomedical Research Institute (NSBRI) through NASA NCC 9-58, as well as NIH R21-EB002416. The authors would like to thank Chen Hui and Liu Zhonghua for their help with technology development, Solomon G. Diamond for the helpful discussion of quantification of motion resistance, Dr. Erika Wagner, Dr. Thomas Zeffiro, and Dan Buckland for their extensive assistance coordinating and conducting the parabolic flight experiment, and Dr. Stuart Harris, Erika Williams, Michael Patz and all of Team Uhuru for their help in data acquisition during the ascent of Mt. Kilimanjaro.

References

- N. J. Holter, "New method for heart studies continuous electrocardiography of active subjects," *Science* **134**, 1214–1220 (1961).
- A. Taddei, G. Distanti, M. Emdin, P. Pisani, G. B. Moody, C. Zeelenberg, and C. Marchesi, "The European ST-T database: standard for evaluating systems for the analysis of ST-T changes in ambulatory electrocardiography," *Eur. Heart J.* **13**(9), 1164–1172 (1992).
- M. W. Martinez, K. J. Rodysill, and T. I. Morgenthaler, "Use of ambulatory overnight oximetry to investigate sleep apnea in a general internal medicine practice," *Mayo Clin. Proc.* **80**(4), 455–462 (2005).
- A. Covic, A. A. Haydar, and D. Goldsmith, "Ambulatory blood pressure monitoring in hemodialysis patients: a critique and literature review," *Semin Dial* **17**(4), 255–259 (2004).
- A. Shoeb, H. Edwards, J. Connolly, B. Bourgeois, S. T. Treves, and J. Guttag, "Patient-specific seizure onset detection," *Epilepsy Behav.* **5**(4), 483–498 (2004).
- S. Schachter, A. Shoeb, A. Bourgeois, S. T. Treves, and J. Guttag, "Feasibility of detecting seizure onsets in ambulatory patients: Initial implementation," *Epilepsia* **46**(suppl 8), 321–322 (2005).
- N. Shinoura and R. Yamada, "Dizziness is associated with decreased vasoreactivity in right cerebral hemisphere for head-down manoeuvre - near-infrared spectroscopy study," *Clin. Physiol. Funct. Imaging* **25**(1), 16–19 (2005).
- E. Szufiadowicz, R. Maniewski, E. Kozluk, A. Zbiec, A. Nosek, and F. Walczak, "Near-infrared spectroscopy in evaluation of cerebral oxygenation during vasovagal syncope," *Physiol. Meas.* **25**(4), 823–836 (2004).
- E. Watanabe, Y. Nagahori, and Y. Mayanagi, "Focus diagnosis of epilepsy using near-infrared spectroscopy," *Epilepsia* **43**, 50–55 (2002).
- E. Watanabe, A. Maki, F. Kawaguchi, Y. Yamashita, H. Koizumi, and Y. Mayanagi, "Noninvasive cerebral blood volume measurement during seizures using multichannel near infrared spectroscopic topography," *J. Biomed. Opt.* **5**(3), 287–290 (2000).
- M. A. Franceschini, D. A. Boas, A. Zourabian, S. G. Diamond, S. Nadgir, D. W. Lin, J. B. Moore, and S. Fantini, "Near-infrared spectroscopy: noninvasive measurements of venous saturation in piglets and human subjects," *J. Appl. Physiol.* **92**(1), 372–384 (2002).
- J. J. van Lieshout, W. Wieling, J. M. Karemaker, and N. H. Secher, "Syncope, cerebral perfusion, and oxygenation," *J. Appl. Physiol.* **94**(3), 833–848 (2003).
- S. C. Schachter, J. Guttag, S. J. Schiff, D. L. Schomer, and Summit Contributors, "Advances in the application of technology to epilepsy: the CIMIT/NIO Epilepsy Innovation Summit," *Epilepsy & Behavior* **16**, 3–46 (2009).
- R. T. Higashida and A. J. Furlan, "Trial design and reporting standards for intra-arterial cerebral thrombolysis for acute ischemic stroke," *Stroke* **34**(8), E109–E137 (2003).
- A. Yodh and B. Chance, "Spectroscopy and imaging with diffusing light," *Phys. Today* **48**(3), 34–40 (1995).
- D. A. Boas, D. H. Brooks, E. L. Miller, C. A. DiMarzio, M. Kilmer, R. J. Gaudette, and Q. Zhang, "Imaging the body with diffuse optical tomography," *IEEE Signal Process. Mag.* **18**(6), 57–75 (2001).
- M. Wolf, M. Ferrari, and V. Quaresima, "Progress of near-infrared spectroscopy and topography for brain and muscle clinical applications," *J. Biomed. Opt.* **12**(6), 062104 (2007).
- Y. Hoshi, "Functional near-infrared spectroscopy: Current status and future prospects," *J. Biomed. Opt.* **12**(6), 062106 (2007).
- B. Chance, Q. M. Luo, S. Nioka, D. C. Alsop, and J. A. Detre, "Optical investigations of physiology: A study of intrinsic and extrinsic biomedical contrast," *Philos. Trans. R. Soc. London, Ser. B* **352**(1354), 707–716 (1997).
- Q. Zhang, H. Ma, S. Nioka, and B. Chance, "Study of near infrared technology for intracranial hematoma detection," *J. Biomed. Opt.* **5**(2), 206–213 (2000).
- <http://www.infrascanner.com/>.
- T. Shiga, K. Yamamoto, K. Tanabe, Y. Nakase, and B. Chance, "Study of an algorithm based on Model experiments and diffusion theory for a portable tissue oximeter," *J. Biomed. Opt.* **2**, 154–161 (1997).
- H. O. Hisaeda, M. Shinohara, M. Kouzaki, and T. Fukunaga, "Effect of local blood circulation and absolute torque on muscle endurance at two different knee-joint angles in humans," *Eur. J. Appl. Physiol.* **86**(1), 17–23 (2001).
- Y. Hoshi, "Functional near-infrared optical imaging: Utility and limitations in human brain mapping," *Psychophysiology* **40**(4), 511–520 (2003).
- Y. Hoshi and S.-J. Chen, "New dimension of cognitive neuroscience research with near-infrared spectroscopy: Free-motion neuroimaging studies," in *Progress in Brain Mapping Research*, F. J. Chen, Ed., pp. 205–229, Nova Science, New York (2006).
- T. Muehleman, D. Haensse, and M. Wolf, "Wireless miniaturized in-vivo near infrared imaging," *Opt. Express* **16**(14), 10323–10330 (2008).
- http://www.artinis.com/index_porti.htm.
- H. Atsumori, M. Kiguchi, A. Obata, H. Sato, T. Katura, T. Funane, and A. Maki, "Development of wearable optical topography system for mapping the prefrontal cortex activation," *Rev. Sci. Instrum.* **80**(4), 043704 (2009).
- H. Atsumori, M. Kiguchi, T. Katura, T. Funane, A. Obata, H. Sato, T. Manaka, M. Iwamoto, A. Maki, H. Koizumi, and K. Kubota, "Noninvasive imaging of prefrontal activation during attention-demanding tasks performed while walking using a wearable optical topography system," *J. Biomed. Opt.* **15**(4), 046002 (2010).
- Q. Zhang, G. E. Strangman, and G. Ganis, "Adaptive filtering to reduce global interference in non-invasive NIRS measures of brain activation: How well and when does it work?," *Neuroimage* **45**(3), 788–794 (2009).
- Q. Zhang, E. N. Brown, and G. E. Strangman, "Adaptive filtering to reduce global interference in evoked brain activity detection: A human subject case study," *J. Biomed. Opt.* **12**(6), 064009 (2007).

32. Q. Zhang, E. N. Brown, and G. E. Strangman, "Adaptive filtering for global interference cancellation and real time recovery of evoked brain activity: A Monte Carlo simulation study," *J. Biomed. Opt.* **12**(4), 044014 (2007).
33. G. Bonmassar, P. L. Purdon, I. P. Jaaskelainen, K. Chiappa, V. Solo, E. N. Brown, and J. W. Belliveau, "Motion and ballistocardiogram artifact removal for interleaved recording of EEG and EPs during MRI," *Neuroimage* **16**(4), 1127–1141 (2002).
34. G. E. Strangman, Q. Zhang, and T. A. Zeffiro, "Near-infrared neuroimaging with NinPy," *Frontiers in Neuroinformatics* **3**, 12 (2009).
35. D. A. Boas, T. Gaudette, G. Strangman, X. Cheng, J. J. A. Marota, and J. B. Mandeville, "The accuracy of near infrared spectroscopy and imaging during focal changes in cerebral hemodynamics," *NeuroImage* **13**, 76–90 (2001).
36. G. Strangman, M. A. Franceschini, and D. A. Boas, "Factors affecting the accuracy of near-infrared spectroscopy concentration calculations for focal changes in oxygenation parameters," *Neuroimage* **18**(4), 865–879 (2003).
37. D. T. Delpy, M. Cope, P. van der Zee, S. Arridge, S. Wray, and J. Wyatt, "Estimation of optical pathlength through tissue from direct time of flight measurement," *Phys. Med. Biol.* **33**, 1433–1442 (1988).
38. A. Villringer and B. Chance, "Non-invasive optical spectroscopy and imaging of human brain function," *Trends Neurosci.* **20**(10), 435–442 (1997).
39. Q. Zhang, T. J. Brukilacchio, A. Li, J. J. Stott, T. Chaves, T. Wu, M. Chorlton, E. Rafferty, R. H. Moore, D. B. Kopans, and D. A. Boas, "Coregistered tomographic x-ray and optical breast imaging: initial results," *J. Biomed. Opt.* **10**(2), 024033 (2005).
40. A. N.S., *American National Standard for Safe Use of Lasers*, American National Standards Institute, New York, New York (1993).
41. Q. Zhang, T. J. Brukilacchio, T. Gaudette, L. Wang, A. Li, and D. A. Boas, presented at the Optical Tomography and Spectroscopy of Tissue IV, San Jose (2001) (unpublished).
42. F. P. Tiecks, A. M. Lam, B. F. Matta, S. Strebel, C. Douville, and D. W. Newell, "Effects of the valsalva maneuver on cerebral circulation in healthy adults. A transcranial Doppler Study," *Stroke* **26**(8), 1386–1392 (1995).
43. R. Looga, "The Valsalva manoeuvre—cardiovascular effects and performance technique: a critical review," *Respir. Physiol. Neurobiol.* **147**(1), 39–49 (2005).
44. R. Saager and A. Berger, "Measurement of layer-like hemodynamic trends in scalp and cortex: implications for physiological baseline suppression in functional near-infrared spectroscopy," *J. Biomed. Opt.* **13**(3), 034017 (2008).
45. L. D. Tripp, J. S. Warm, G. Matthews, P. Y. Chiu, and R. B. Bracken, "On tracking the course of cerebral oxygen saturation and pilot performance during gravity-induced loss of consciousness," *Human Factors* **51**(6), 775–784 (2009).
46. B. S. Shender, E. M. Forster, L. Hrebien, H. C. Ryoo, and J. P. Cammarota, Jr., "Acceleration-induced near-loss of consciousness: the 'A-LOC' syndrome," *Aviat. Space Environ. Med.* **74**(10), 1021–1028 (2003).
47. J. Engel, Jr., T. A. Pedley, J. Aicardi, M. A. Dichter, and S. Moshé, *Epilepsy: A Comprehensive Textbook*, Lippincott-Raven, Philadelphia (2007).
48. J. K. Russell and S. Gehman, "Early experience with a novel ambulatory monitor," *J. Electrocardiol.* **40**(6), S160–S164 (2007).